Subnanometer optical coherence tomographic vibrography

Ernest W. Chang,[1,2] James B. Kobler,[3] and Seok H. Yun[1,*]

[1]*Harvard Medical School and Wellman Center for Photomedicine, Massachusetts General Hospital, 40 Blossom Street, Boston, Massachusetts 02114, USA*

[2]*Department of Biomedical Engineering, Boston University, 44 Cummington Street, Boston, Massachusetts 02115, USA*

[3]*Center for Laryngeal Surgery and Voice Rehabilitation, Massachusetts General Hospital, 70 Blossom Street, Boston, Massachusetts 02114, USA*

**Corresponding author: syun@hms.harvard.edu*

Received April 20, 2012; revised July 18, 2012; accepted July 19, 2012; posted July 19, 2012 (Doc. ID 167161); published August 29, 2012

The ability to quantify and visualize submicrometer-scale oscillatory motions of objects in three dimensions has a wide range of application in acoustics, materials sciences, and medical imaging. Here we demonstrate that volumetric snapshots of rapid periodic motion can be captured using optical coherence tomography (OCT) with subnanometer-scale motion sensitivity and microsecond-scale temporal resolution. This technique, termed OCT vibrography, was applied to generate time-resolved volumetric vibrographs of a miniature drum driven acoustically at several kilohertz. © 2012 Optical Society of America

OCIS codes: 110.0110, 120.0120, 120.7280, 170.4500.

Pressure-driven oscillations with nanometer-scale amplitudes at acoustic frequencies are found in a variety of physical and biological measurement systems. For instance, miniature resonators have been used for radiation pressure cooling [1], the sensing of molecules [2], and the high-precision weighing of single cells [3]. Moreover, acoustic vibrations have been used for dynamic mechanical analysis and rheology and for photoacoustic imaging [4] and elastography. In all of these systems, measurements of the acoustic motion on the surface or within the object are essential. Although the identification of the intrinsic parameters, such as the resonance frequency, is sufficient for some cases, other applications require the actual amplitude and phase information, and such applications can greatly benefit from a volumetric imaging technique capable of providing spatial graphs—"vibrographs"—of the sample vibration.

Optical interferometry is ideally suited for precise measurements of oscillatory motion. Laser Doppler velocimetry and stroboscopic holography have been used to measure submicrometer-scale vibrations at frequencies up to megahertz [5]. However, these techniques are limited to surface measurements. Optical coherence tomography (OCT) offers the potential for capturing motion at various depths in scattering samples. Phase-sensitive OCT with subnanometer amplitude sensitivity has been used for elastography [6–8], vibration-amplitude mapping [9], and phase microscopy of static or slowly moving samples [10,11].

Here, we demonstrate a new technique capable of providing reconstructed volumetric snapshots of rapidly moving samples. This technique, which we call OCT vibrography, is based on the synchronized acquisition of phase information that is directly related to the vibration of the sample. After post-processing, three-dimensional (3D) snapshots of an object vibrating at acoustic frequencies in response to applied stimuli could be obtained. We show that OCT vibrography using a wavelength-swept laser source can achieve subnanometer amplitude sensitivity by minimizing mechanical noise associated with laser tuning and beam scanning. For a proof-of-concept experiment, we applied OCT vibrography to the visualization of the acoustic resonance modes of a membrane.

Figure 1 shows the schematic of our experimental setup used to measure vibrations. The OCT console was an optical frequency domain imaging system based on a wavelength-swept source [12]. The sample was a glass plate mounted on a piezoelectric transducer (PZT; AE0203D08F, Thorlabs). Sinusoidal waveforms from a function generator (33120A, Agilent) were used to drive the PZT actuator. A multifunctional board (DAQ; PCI 6115, National Instruments) was used to acquire interference data at 10 MS/s and control the polygon filter of the laser source to generate a 15–20 kHz A-line rate. The tuning range of the laser was 125 nm with a mean wavelength of 1280 nm. The DAQ board also produced an analog output (16 bit) to control a two-axis galvanometer beam scanner (6210H, Cambridge Technologies) and provided a transistor–transistor logic trigger signal to the function generator. By generating all control signals from the internal time-base clock (20 MHz) of the DAQ

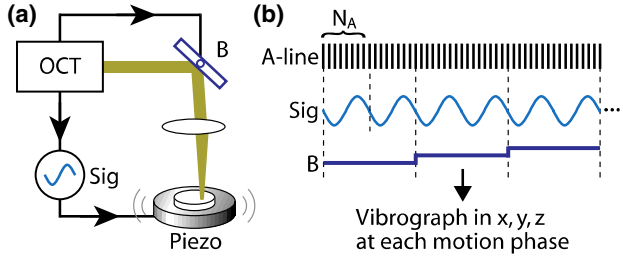

Fig. 1. (Color online) (a) Schematic of a system. Sig, signal generator; *B*, galvanometer beam scanner. (b) Schematic of synchronized data acquisition. A number of A-lines, N_A, are acquired during each cycle of oscillation, while the scanner (*B*) is parked at a spatial location for the duration of a user-controlled number of motion cycles (Sig). An arrangement of the data with respect to time generates vibrographs at each motion phase.

board, we achieved synchronization among data acquisition, beam scanning, and sample actuation.

The frequency of the driving sinusoidal waveform (Sig) was set at an integer fraction of the A-line rate (15–20 kHz), so that an integer number of A-lines, N_A, were acquired during each cycle of sample oscillation. N_A also represents the number of motion phases captured in a cycle. The beam scan was synchronized to the oscillation so that after a predetermined number of cycles, N_B, the beam was stepped to the next lateral location using the galvanometer beam scanner (B). The lowest possible N_A and N_B are 2 and 1, respectively, where two motion phases are captured per cycle (Nyquist limit) and the beam is moved after the completion of each vibration cycle. However, $N_A > 6$ is highly desirable to accurately reconstruct the sinusoidal motion in terms of amplitude and phase. Figure 1(b) illustrates a case for $N_A = 8$ and $N_B = 2$. When the scans over the regions of interest in the sample were completed, the A-line profiles acquired at the same phase of the oscillation ($\varphi = 0, 2\pi/N_A, \ldots$ or $2\pi(N_A - 1)/N_A$) were grouped to produce "snapshots" [13] or vibrographs of the sample.

The intensity and phase of the interference signals from a specific location in the external and internal surfaces of the sample were measured during the oscillatory motion. The phase angle, ϕ, can be expressed as $\phi(t) = \Delta\phi \sin(2\pi f t) + \phi_n$, where $\Delta\phi = 4\pi/\lambda * \delta z$ is the phase amplitude corresponding to the vibration amplitude δz (in nanometers), f is the vibration frequency, and ϕ_n is the intrinsic phase noise given by $\langle \delta\phi_n \rangle^2 = 1/(2 * \mathrm{SNR})$, where SNR is the signal-to-noise ratio for the intensity of the interference signal in a single A-line [14]. When the vibration amplitude is determined from N A-lines, the amplitude sensitivity is given by $\lambda/4\pi(2 * \mathrm{SNR} * N)^{-1/2}$, where $N = N_A$ for single-cycle measurement, and $N = N_A * N_B$ for averaging over N_B cycles [6–9]. Spatial averaging over multiple points in a region where the motion is uniform can further enhance the sensitivity.

To reach the SNR-limited sensitivity, it was found to be essential to isolate the measurement system from room acoustic noise and mechanical noises, such as the vibration of the rotating polygon filter of the laser, using vibration absorbing platforms and pads made with low resonant frequency (15 Hz) viscoelastic sorbothane polymer. We also found it necessary to reduce the amplitude jitter (1–5 nm in amplitude) from the galvanometer scanner [11]. The noise from the scanner was due to its finite frequency response. We canceled out this deterministic noise in real time by numerically subtracting a prerecorded trace of the scanner's step response measured from a stationary sample. We estimate the total residual mechanical noise to be <20 pm.

To test the sensitivity of the OCT system, we imaged a sample vibrating at 1.5 kHz with an A-line rate of 15 kHz. The amplitude of vibration was measured to be 7 nm, as confirmed with a laser Doppler velocimeter. We measured the phase angle of the OCT pixel corresponding to the top surface of the glass plate while the beam was fixed. The SNR of the pixel was 30 dB. Figure 2(a) (inset) shows a typical time trace of the phase angle. The spectrum in Fig. 2(a) shows the Fourier domain trace of the measured phase angles ($N = 2880$; $N_A = 10$, $N_B = 288$), showing a sample vibration peak at 1.5 kHz and a noise floor of 46 pm, close to the theoretical limit of 42 pm. The SNR was varied using a graded neutral density filter to explore the relationship between the SNR and sensitivity. Then, we measured the average of the random phase variation in a group of A-lines to calculate the amplitude sensitivity. Figure 2(b) shows the vibration sensitivity at SNR levels ranging from 20 to 40 dB for different numbers ($N = 1$ to 1000) of A-lines averaged. In all cases, SNR-limited theoretical sensitivity was obtained. At SNR = 40 and $N = 1000$ (integration time, 0.667 s), the sensitivity was 26 pm.

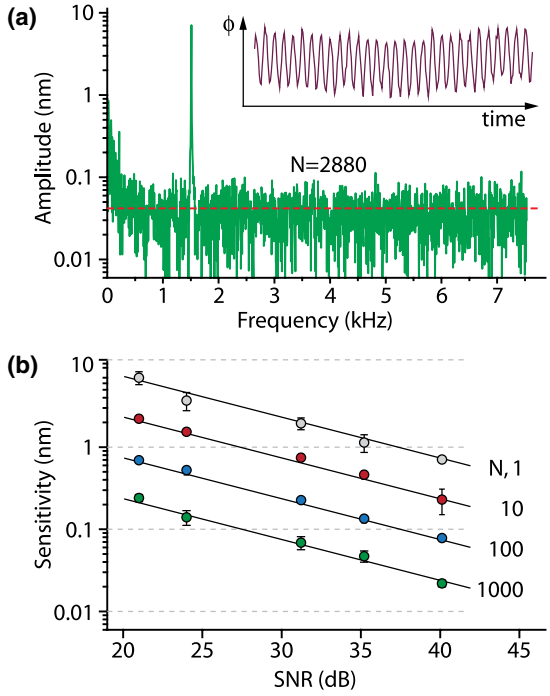

Fig. 2. (Color online) (a) Inset is the representative time trace of the measured phase angle. Fourier domain spectrum of the PZT vibration of 288 cycles. The peak points to the vibration frequency of 1.5 kHz. (b) Sensitivity measurement of OCT vibrography. Circles, experimental data for $N = 1$, 10, 100, and 1000; error bars, s.d; lines, theoretical curves for SNR-limited sensitivity.

We next used the vibrography system to capture 3D snapshots of an acoustically driven drum head consisting of a 200-μm-thick latex membrane stretched over and glued to a 5 mm diameter metal tube (Fig. 3(a)). Sinusoidal signals from the function generator were applied to a loudspeaker, and the radiated sound was used to evoke the vibration of the drumhead. The OCT beam was scanned over the entire membrane ($N_B = 1$), covering 512 by 256 XY spatial points. The SNR at the drum surface was approximately 40 dB. By sweeping the sound frequency, we found a resonance at 800 Hz for the fundamental resonance mode, the (0, 1) mode, where the maximum displacement was observed. Figure 3(b) shows snapshots of the membrane taken at two opposite vibration phases, $\varphi = 0$ and π, respectively, at $f = 800$ Hz ($N_A = 20$; A-line rate was 16 kHz). The cutaway view reveals the homogeneous vibration across the full thickness of the latex membrane (Fig. 3(c)). A movie created from the snapshots shows the Bessel profile of the vibration mode with a 3D spatial resolution of approximately

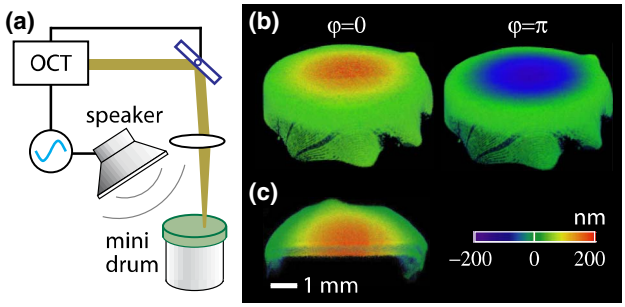

Fig. 3. (Color online) (a) Schematic of setup with a latex drum, (b) vibrography snapshot images (0 and π motion phases) of the vibrating drum at the fundamental frequency of 800 Hz (Media 1), and (c) a cutaway image showing the motion in a cross-section of the membrane.

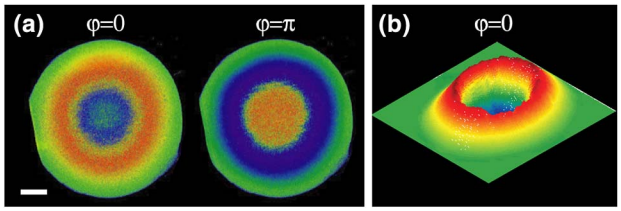

Fig. 4. (Color online) (a) Snapshot vibrographs of the drumhead (0 and π motion phases) at 1.78 kHz. At this frequency, the second-order mode was predominantly produced (Media 2). Scale bar, 1 mm. (b) A 3D contour graph.

10 μm and a motion-phase resolution of $2\pi/20$ (Media 1). It took 163.8 s to acquire the full 3D data set (512 by 256 by 400 pixels in XYZ and 20 motion phases).

As the sound frequency was increased, we observed higher-order vibration modes. Figure 4(a) shows snapshots of the motion at 1.78 kHz ($N_A = 9$), when the resonant excitation of the second-order radial mode, the (0,2) mode, became evident. The ratio of the resonance frequencies between the first and second radial modes was close to 2.3, as expected from acoustic theory [15]. Figure 4(b) shows a 3D contour plot, which highlights the characteristic amplitude pattern of the second-order radial mode. A movie created from the snapshots shows the profile of the vibration mode with a motion-phase resolution of $2\pi/9$ (Media 2). The data acquisition time was 73.6 s.

We have described a synchronized OCT system capable of visualizing the acoustic vibrations. The maximum frequency was approximately 3 kHz, only limited by the finite A-line rate (20 kHz) of the current system. With a higher A-line rate, the range could be extended by an order of magnitude. The lower limit of the frequency range is primarily determined by considering the overall data acquisition time, as the acquisition time is proportional to the inverse of the frequency times the number of spatial points in XY. For frequencies below 100 Hz, the data acquisition and scanning sequence shown in Fig. 1(b) may no longer be optimal, and a modified sequence could reduce the data acquisition time (e.g., $N_A = 8$ is sufficient to obtain a subnanometer sensitivity at SNR of >30 dB; see Fig. 2(b)). Time synchronization and mechanical noise reduction enabled us to obtain the subnanometer displacement sensitivity. We expect that OCT vibrography can be used to visualize the vibrational modes of optomechanical devices for fundamental and applied studies. OCT vibrography may allow a new approach in dynamic rheometry. Another area of application is evaluating the function of the tympanic membrane, ossicles, and inner ear [16] in response to sound.

We thank J. J. Rosowski and J. T. Cheng for discussion. This work was funded by the National Institutes of Health (P41EB015903, U54CA143837).

References

1. D. Kleckner and D. Bouwmeester, Nature **444**, 75 (2006).
2. T. J. Kippenberg and K. J. Vahala, Opt. Express **15**, 17172 (2007).
3. T. P. Burg, M. Godin, S. M. Knudsen, W. Shen, G. Carlson, J. S. Foster, K. Babcock, and S. R. Manalis, Nature **446**, 1066 (2007).
4. M. H. Xu and L. H. V. Wang, Rev. Sci. Instrum. **77**, 041101 (2006).
5. J. T. Cheng, A. A. Aarnisalo, E. Harrington, M. D. Hernandez-Montes, C. Furlong, S. N. Merchant, and J. J. Rosowski, Hearing Res. **263**, 66 (2010).
6. X. Liang, M. Orescanin, K. S. Toohey, M. F. Insana, and S. A. Boppart, Opt. Lett. **34**, 2894 (2009).
7. B. F. Kennedy, X. Liang, S. G. Adie, D. K. Gerstmann, B. C. Quirk, S. A. Boppart, and D. D. Sampson, Opt. Express **19**, 6623 (2011).
8. R. K. Chhetri, K. A. Kozek, A. C. Johnston-Peck, J. B. Tracy, and A. L. Oldenburg, Phys. Rev. E **83**, 040903 (2011).
9. R. K. Wang and A. L. Nuttall, J. Biomed. Opt. **15**, 056005 (2010).
10. M. A. Choma, A. K. Ellerbee, C. H. Yang, T. L. Creazzo, and J. A. Izatt, Opt. Lett. **30**, 1162 (2005).
11. C. Joo, T. Akkin, B. Cense, B. H. Park, and J. E. de Boer, Opt. Lett. **30**, 2131 (2005).
12. S. H. Yun, G. J. Tearney, J. F. de Boer, N. Iftimia, and B. E. Bouma, Opt. Express **11**, 2953 (2003).
13. E. W. Chang, J. B. Kobler, and S. H. Yun, Sci. Rep. **1**, 48 (2011).
14. B. J. Vakoc, S. H. Yun, J. F. de Boer, G. J. Tearney, and B. E. Bouma, Opt. Express **13**, 5483 (2005).
15. R. S. Christian, R. E. Davis, A. Tubis, C. A. Anderson, R. I. Mills, and T. D. Rossing, J. Acoust. Soc. Am. **76**, 1336 (1984).
16. F. Y. Chen, D. J. Zha, A. Fridberger, J. F. Zheng, N. Choudhury, S. L. Jacques, R. K. Wang, X. R. Shi, and A. L. Nuttall, Nat. Neurosci. **14**, 770 (2011).